Coordination of NMCP1- and NMCP2-class proteins within the plant nucleoskeleton

Endia L. Blunt[a,b], Jason A. Shandler[c], Erika J. Hughes[a], Hayley Sussman[a], Rachel C. Christopherson[d], and Eric J. Richards[a,b,*]

[a]Boyce Thompson Institute, Ithaca, NY 14853; [b]Department of Molecular Biology and Genetics, Cornell University, Ithaca, NY 14853; [c]College of Agriculture and Life Sciences and [d]College of Arts & Sciences, Cornell University, Ithaca, NY 14853

ABSTRACT **Plants lack lamin proteins but contain a class of coiled-coil proteins that serve as analogues to form a laminal structure at the nuclear periphery. These nuclear matrix constituent proteins (NMCPs) play important roles in regulating nuclear morphology and are partitioned into two distinct groups. We investigated *Arabidopsis* NMCPs (called CRWNs) to study the interrelationship between the three NMCP1-type paralogues (CRWN1, 2, and 3) and the lone NMCP2-type paralogue, CRWN4. An examination of *crwn* mutants using protein immunoblots demonstrated that CRWN4 abundance depends on the presence of the NMCP1-type proteins, particularly CRWN1. The possibility that CRWN4 is coimported into the nucleus with nuclear localization signal (NLS)-bearing paralogues in the NMCP1-clade was discounted based on recovery of a *crwn4-2* missense allele that disrupts a predicted NLS and lowers the abundance of CRWN4 in the nucleus. Further, a screen for mutations that suppress the effects of the *crwn4-2* mutation led to the discovery of a missense allele, *impa-1*^{G146E}, in one of the nine importin-α genes in the *Arabidopsis* genome. Our results indicate that the CRWN4 carries a functional NLS that interacts with canonic nuclear import machinery. Once imported, the level of CRWN4 within the nucleus is modulated by the abundance of NMCP1 proteins.**

Monitoring Editor
Tom Misteli
National Institutes of Health, NCI

Received: Aug 22, 2019
Revised: Sep 21, 2020
Accepted: Oct 27, 2020

INTRODUCTION

Regulation of nuclear morphology in plants results from signaling and physical interactions that span the nuclear envelope. A conserved complex, called the linker of the nucleoskeleton and cytoskeleton (LINC) (Padmakumar *et al.*, 2005; Crisp *et al.*, 2006; Horn, 2014; Meier *et al.*, 2017), serves as a bridge between the cytoskeleton and architectural elements within the nucleus. A key structural element within the nucleus is the nuclear lamina (Gruenbaum *et al.*, 2005; Dechat *et al.*, 2008), which lines the inner nuclear membrane and provides mechanical stability for the nucleus (Lammerding *et al.*, 2004; Lammerding, 2011). In plants, one component of the nuclear lamina consists of a family of plant-specific nuclear coiled-coil proteins, which were originally identified as nuclear matrix constituent proteins (NMCPs) in carrot (Masuda *et al.*, 1993, 1997, 1999; Ciska *et al.*, 2013). This protein family separates into two major phylogenetic clades, named the NMCP1-like and NMCP2-like clades (Kimura *et al.*, 2010), and most plant species contain at least one homologue from each group (Poulet *et al.*, 2017; Ciska *et al.*, 2019).

The *Arabidopsis* genome contains four genes encoding NMCP-like proteins, including three NMCP1 homologues (called CRWN1, 2, and 3 in *Arabidopsis*) and one NMCP2 orthologue (CRWN4) (Dittmer *et al.*, 2007; Sakamoto and Takagi, 2013; Wang *et al.*, 2013). Studies of fusion protein localization in transgenic plants indicate that CRWN1 and CRWN4 are concentrated at the nuclear periphery, while CRWN2 and CRWN3 are distributed more broadly throughout the *Arabidopsis* nuclei (Dittmer *et al.*, 2007; Dittmer and Richards, 2008; Sakamoto and Takagi, 2013). Our previous work with loss-of-function alleles for each CRWN protein determined that at least one functional CRWN protein is required for plant viability (Wang *et al.*, 2013). Single *crwn* mutants appear similar to wild type (WT) at the whole-plant level. However, loss of *CRWN1* has a dramatic effect on nuclear morphology, leading to smaller spherical

This article was published online ahead of print in MBoC in Press (http://www.molbiolcell.org/cgi/doi/10.1091/mbc.E19-08-0464) on November 4, 2020.

*Address correspondence to: Eric J. Richards (ejrichards@btiscience.org).

Abbreviations used: EMS, ethylmethansulfonate; NLS, nuclear localization signal; NMCP, nuclear matrix constituent protein; WT, wild type.

nuclei, but loss of either *CRWN2* and/or *CRWN3* does not (Dittmer *et al.*, 2007; Sakamoto and Takagi, 2013; Wang *et al.*, 2013). Loss of *CRWN4* also causes reduced nuclear size and spherical nuclei with additional phenotypes, including dispersal of heterochromatin aggregates and irregular nuclear margins (Sakamoto and Takagi, 2013; Wang *et al.*, 2013). Combining *crwn* mutations leads to further decreases in nuclear size and a reduction in plant stature. Study of the double and triple mutants demonstrated that plants cannot survive with only CRWN1 or only CRWN4, indicating that these proteins have some nonoverlapping functions (Wang *et al.*, 2013). In contrast, CRWN2 and CRWN3 are considered "generalists" that are able to cover the function of both CRWN1 and CRWN4.

Although *crwn1* and *crwn4* mutants result in similar reductions in nuclear size, *crwn4* mutants exhibit more severe phenotypes compared with *crwn1* plants. For example, the degree of transcriptomic changes is higher in *crwn4* mutants (Choi *et al.*, 2019), and chromocenter organization is disrupted in *crwn4* but not *crwn1* nuclei (Wang *et al.*, 2013). In combining these mutations, complex functional interactions between *CRWN1* and *CRWN4* begin to emerge. Nuclear size decreased further, illustrating an additive effect, while these mutations have a synergistic effect on whole-plant morphology (e.g., *crwn1 crwn4* plants are semidwarf) (Wang *et al.*, 2013). Antagonistic effects were also exhibited; for example, *crwn1 crwn4* mutants show less severe gene misexpression (Choi *et al.*, 2019) and more normal chromocenter organization relative to *crwn4* single mutants (Wang *et al.*, 2013). We hypothesize that physical interactions, either direct or indirect, among CRWN paralogues might mediate these complex functional interactions. Additional support for this hypothesis comes from coimmunoprecipitation experiments that demonstrated that CRWN1 and CRWN4 are found together with other proteins in large macromolecular complexes (Goto *et al.*, 2014; Mikulski *et al.*, 2019). In this study, we address how the activities of NMCP1- and NMCP2-type proteins are coordinated in the nucleus.

RESULTS

The four *Arabidopsis* CRWN proteins exhibit a tripartite domain structure characteristic of NMCP proteins, consisting of a large, central coiled-coil domain flanked by a short N-terminal and a longer C-terminal domain (Figure 1A). The size and amino acid sequence of the N-termini are variable among CRWN paralogues (Figure 1B), with CRWN2 and CRWN3 sharing the highest similarity (approximately 30% identity). Paralogues of the CRWN1-like clade have a conserved approximately 20-amino-acid block at the end of the C-terminus that is absent in CRWN4 and NMCP2-like members from other species (blue regions, Figure 1A). CRWN1, CRWN2, and CRWN3 also contain two conserved monopartite nuclear localization signals (NLSs) within the C-terminal region, including an associated YNL sequence motif (Figure 1C). Kimura *et al.* (2014) demonstrated that this motif and the neighboring NLSs (termed NLSm3 and NLSm4) in carrot NMCP1 function to specify nuclear localization. By comparison, carrot NMCP2 and *Arabidopsis* CRWN4 lack these motifs. However, CRWN4 contains a predicted monopartite NLS (purple region, Figure 1, A and D), as well as an overlapping predicted bipartite NLS, in a comparable position approximately 120 amino acids from the C-terminus.

Nuclear accumulation of CRWN4 depends on the presence of CRWN1 and CRWN3

To probe the size and abundance of CRWN protein paralogues, we developed antibodies to detect these proteins by exploiting the amino acid divergence in their N-terminal regions. We focused on CRWN1 and CRWN4 as the representatives of the two main NMCP clades and generated anti-peptide polyclonal antisera in rabbits that recognize epitopes within the N-terminus of CRWN1 and CRWN4 (underlined peptides in Figure 1B). To test whether these antibodies detected our proteins of interest, we prepared nuclear extracts from seedling tissue and size fractionated the proteins by SDS–PAGE and performed protein blot analysis using the anti-CRWN peptide antisera (Supplemental Figure S1). Three different genotypes were used in these validation experiments: WT and two homozygous mutants, *crwn1-1* and *crwn4-1*, each carrying a null allele (T-DNA insertion in the Columbia background) that blocks the production of a full-length transcript (Dittmer *et al.*, 2007; Wang *et al.*, 2013). When we probed with the anti-CRWN1 antisera, three bands were detected, migrating with apparent molecular weights of between 100 and 250 kDa in the WT and *crwn4-1* samples. The most intense band migrated at about 110 kDa; the predicted size of the CRWN1 is 129 kDa. The anti-CRWN4 antibody detected two bands in the WT and *crwn1-1* samples, with the strongest at approximately 140 kDa, in reasonable agreement with CRWN4's predicted size of 121 kDa. No bands were detected in the *crwn1-1* and *crwn4-1* samples by their cognate antibodies, indicating that each antibody is specific for its intended epitope target. The presence of multiple bands for CRWN1 and CRWN4 could be due to posttranslational modifications, proteolytic processing, and/or degradation during preparation of the nuclear extracts.

These antibody reagents allowed us to investigate the interdependence of the different CRWN proteins. Specifically, we asked whether there were qualitative or quantitative changes in CRWN protein abundance in the nucleus when one of the four paralogues was missing. To do so, we measured the abundance and size of CRWN1 and CRWN4 species in nuclear extracts prepared from WT and *crwn* single mutant seedlings (Figure 2). As expected, signals in the *crwn1-1* and *crwn4-1* nuclear extract samples were not detected using the CRWN1 and CRWN4 antibodies, respectively, demonstrating the specificity of the antibodies as shown in Supplemental Figure S1. We observed no significant differences in CRWN1 abundance or size across the remaining *crwn* single mutants (Figure 2A). However, the *crwn1-1* and *crwn3-1* nuclear extracts exhibited a reduction in CRWN4 protein abundance compared with that of WT, while the *crwn2-1* sample showed no significant change (Figure 2B). These results indicate that CRWN1 and CRWN3 are needed for normal levels of CRWN4 to accumulate in the nucleus while loss of CRWN2 has no effect on CRWN4 abundance.

CRWN4 mRNA expression is increased in single mutants affecting NMCP1-clade paralogues

As the reduction in CRWN4 abundance could be due to a decrease in expression of *CRWN4* in *crwn1-1* and *crwn3-1* mutants, transcript levels of *CRWN4* in the *crwn* single mutants were examined via quantitative reverse transcriptase (qRT-PCR) analysis (Figure 3). RNA was extracted from WT and *crwn* single mutant seedlings and used to synthesize cDNA, which was then processed as the template in qPCRs. Using the housekeeping genes *ACTIN2* and *UBC* as the normalization controls, we observed an increase in *CRWN4* transcript levels in *crwn1-1*, *crwn2-1*, and *crwn3-1* samples compared with WT. These results indicate that loss of CRWN1, CRWN2, or CRWN3 leads to a modest boost in *CRWN4* expression at the mRNA level. Therefore, the decrease in CRWN4 protein levels within nuclei of *crwn1-1* and *crwn3-1* mutants is not due to down-regulation of the *CRWN4* transcript. Rather, these results indicate that normal levels of CRWN4 accumulation require CRWN1 or CRWN3 at the post-transcriptional or protein level.

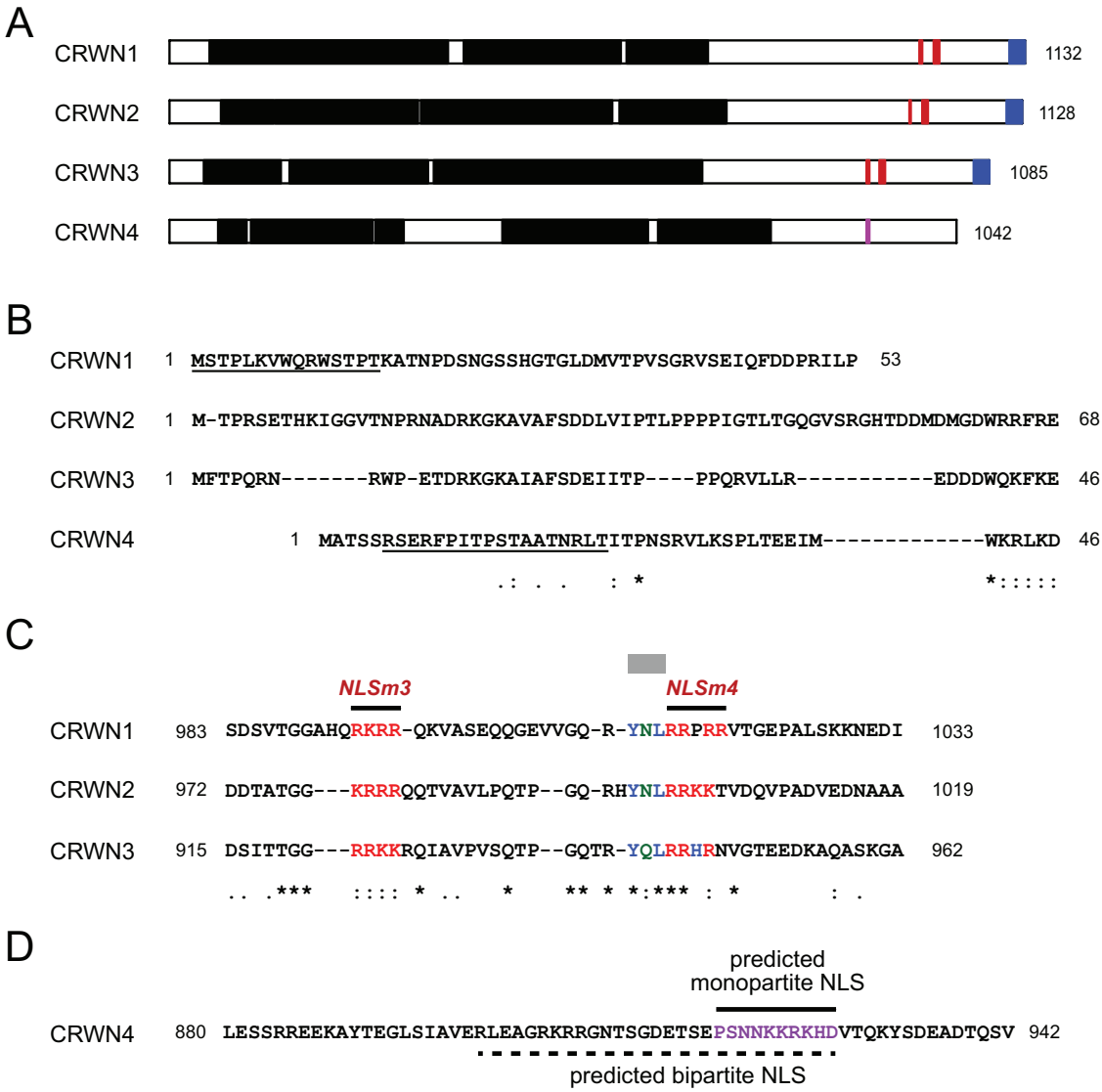

FIGURE 1: The CRWN protein family. (A) The organization of CRWN protein paralogues, specifying the positions of the coiled-coil domains in black, the predicted NLS regions (conserved NMCP1-type motifs in red and predicted motifs in purple), and the NMCP1-type C-terminal domain in blue. Numbers indicate amino acid residues. (B) An amino acid sequence alignment of the N-termini of the four CRWN proteins. The peptide sequences used to raise specific antibodies recognizing CRWN1 and CRWN4 are underlined. (C) The NMCP1-type NLS motifs in red and the associated YNL region (denoted by the gray rectangle) using conventional Clustal color coding. The symbols below the sequence alignments in panels B and C indicate identities (*) or decreasing levels of amino acid conservation (: then.). (D) A corresponding but diverged region of CRWN4 lacks NMCP1-type NLS motifs, yet contains a predicted NLS (purple) and an overlapping predicted bipartite NLS.

The reduction in nuclear CRWN4 abundance in the absence of CRWN1 is enhanced by a deficiency of CRWN2 or CRWN3

We considered two working models to explain why the abundance of CRWN4 in the nucleus is dependent on NMCP1-clade paralogues. One model is that CRWN4 is stabilized by interaction with NMCP1-type proteins or that CRWN4 levels are tuned to that of its paralogues through regulated protein degradation. Another possibility is that CRWN4, which lacks an obvious or at least a well-conserved NLS, requires interaction with an NMCP1-clade protein, which carries a functional NLS motif, for entry into the nucleus. Such a mechanism has some attractive features, such as the ability to balance the stoichiometry of different monomer classes within the nucleus.

To begin exploring these possibilities, CRWN4 abundance was examined using nuclear extracts of the *crwn* double mutants (Figure 4). We observed a dramatic reduction in nuclear CRWN4 levels in *crwn1-1 crwn2-1* and *crwn1-1 crwn3-1* double mutants, suggesting a synergistic effect of combining the *crwn1-1* and *crwn3-1* single mutations. In contrast, only a modest decrease in CRWN4 levels was observed in the *crwn2-1 crwn3-1* double mutant samples. We conclude that the reduction in CRWN4 abundance in the mutant nuclei is caused primarily by the absence of CRWN1 and enhanced by a deficiency of CRWN3 or CRWN2. The synergistic effect of mutations in the CRWN1-like clade on nuclear levels of CRWN4 parallels the effect of these mutation combinations on nuclear size (Dittmer *et al.*, 2007; Wang *et al.*, 2013). These findings are consistent with a stabilization model in which CRWN4 primarily interacts with CRWN1

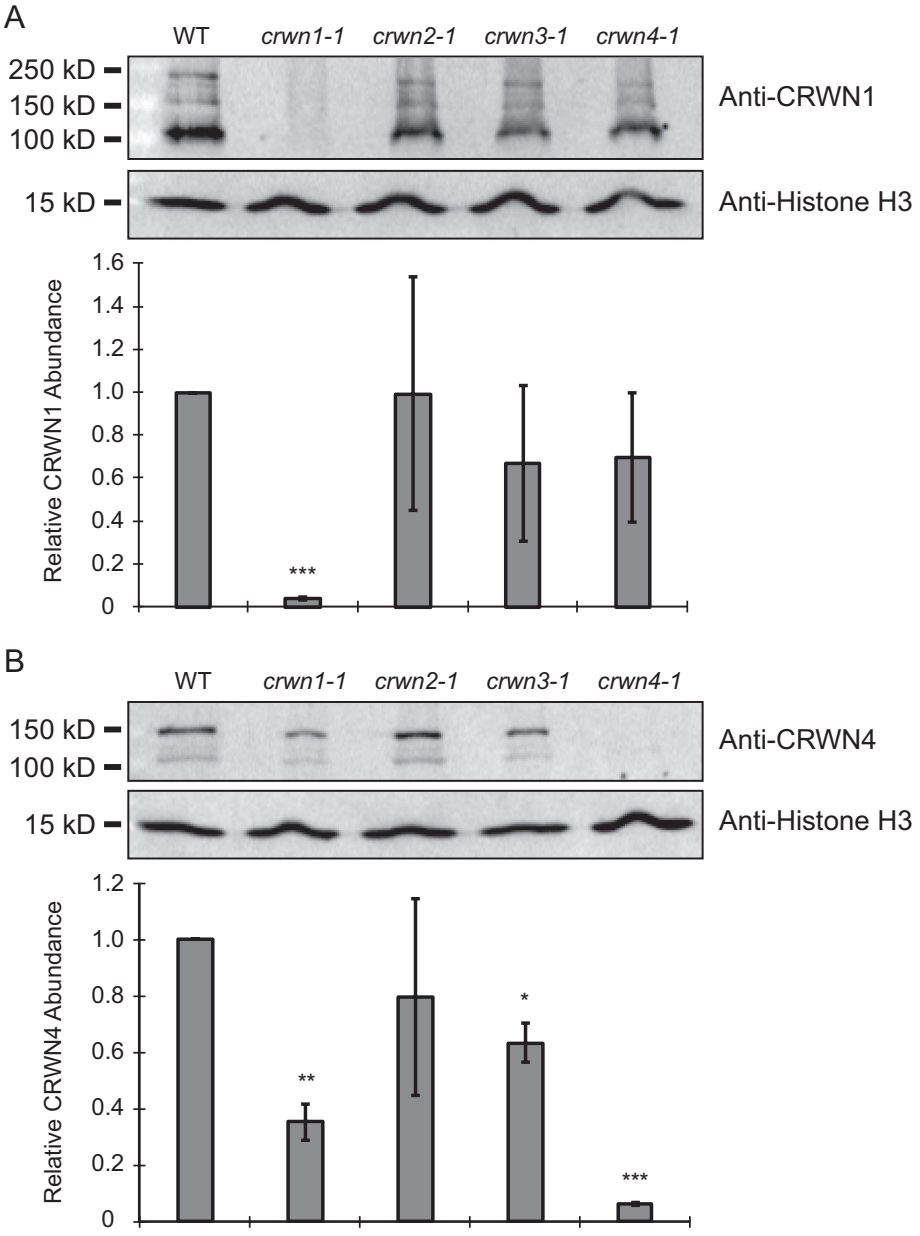

FIGURE 2: CRWN1 and CRWN4 protein abundance in *crwn* single mutants. Protein immunoblots of size-fractionated nuclear extracts obtained from WT and *crwn* single mutant seedlings were incubated with the indicated antibodies (panel A, anti-CRWN1; panel B, anti-CRWN4), and the specific proteins were detected using a standard enhanced chemiluminescence (ECL) protocol after incubation with an HRP-conjugated secondary antibody. The abundance of histone H3 was used as a normalization standard. Quantifications of the chemiluminescence signals were performed using a Storm imager and ImageQuant TL software (Amersham Biosciences), and the averages of two independent experiments ± SD are shown; * represents p value < 0.05; ** represents p value < 0.01; *** represents p value < 0.001.

and then CRWN3, and with CRWN2 to a lesser extent. These results, however, are also consistent with a nuclear coimport mechanism with CRWN4 translocation into the nucleus in partnership with a hierarchy of NMCP1-clade proteins (CRWN1 > CRWN3 > CRWN2).

Discovery of a novel CRWN4 mutation revealing a putative NLS motif

A key premise of the coimport model is that CRWN4 lacks an NLS motif. This premise was challenged by the discovery of a novel missense *crwn4* allele that alters a region with similarity to an NLS. Nuclear localization signals are usually short motifs, consisting of the basic amino acids lysine and arginine, that are recognized by karyopherins (such as importin-α) in the cytoplasm to form complexes targeted for transport into the nucleus (Kosugi *et al.*, 2009a). As noted above, CRWN4 was not previously known to contain a functional NLS, nor were candidate NLS motifs seen in NMCP2 (Kimura *et al.*, 2010) or conserved regions shared among NMCP2-like proteins in other taxa (Ciska *et al.*, 2019). However, a forward genetics screen for abnormal nuclear morphology mutants led to the recovery of a missense allele (designated *crwn4-2*) causing a phenotype resembling that of our well-characterized loss-of-function allele, *crwn4-1*. Compared with WT, the *crwn4-2* mutation results in smaller and more spherical nuclei, as well as reduced chromocenter numbers (typically five chromocenters or fewer in *crwn4-2* nuclei compared with 8–10 in WT) (Figure 5A and Supplemental Figure S2). The *crwn4-2* missense allele is caused by an ApA to CpT change at positions 26315087-8 (TAIR10 annotation of chromosome 5) within the sixth exon of the *CRWN4* gene. This dinucleotide change results in the single-amino-acid change K923L, which lies within a putative NLS motif (PSNNKKRKHD → PSNNLKRKHD; see Figure 1D). We also investigated the nuclear abundance of CRWN4 within this mutant and discovered a significant decrease in CRWN4 levels compared with WT (Figure 5B). These results suggest that CRWN4 contains a functional NLS that is disrupted by the *crwn4-2* mutation. However, we cannot rule out the possibility that the missense mutation leads to increased protein turnover, perhaps due to misfolding and/or an inability to interact with binding partners.

Isolation of an extragenic suppressor of the *crwn4-2* mutation

To gain further insight into the nuclear accumulation of CRWN4, we conducted a genetic screen for second-site mutations that suppress the effects of the *crwn4-2* mutation. Seeds homozygous for *crwn4-2* and a nuclear green fluorescent protein (GFP) marker were mutagenized with ethylmethansulfonate (EMS), and the individuals in the M_2 generation were screened for elongated nuclei in root cells. We discovered one such individual out of a population of nearly 900 M_2 seedlings as a candidate carrying either a reversion mutation or a second-site suppressor mutation. M_3 progeny of this phenotypically suppressed individual also showed elongated nuclei in several tissues. As shown in Figure 5A, 4′,6-diamidino-2-phenylindole (DAPI)-stained anther filament nuclei in phenotypically suppressed M_4 individuals (designated *crwn4-2;*

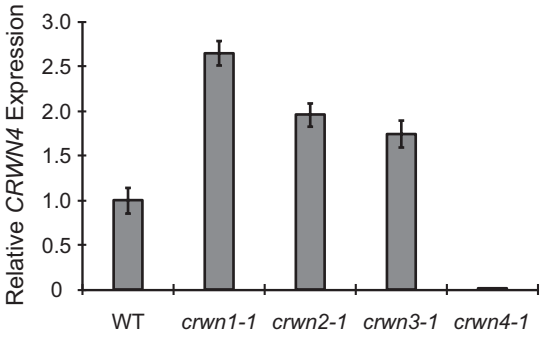

FIGURE 3: *CRWN4* transcript levels are elevated in the absence of individual NMCP1-clade proteins. The expression profile of *CRWN4* was generated by qRT-PCR analysis of transcripts in WT and *crwn* single mutant seedlings. *ACTIN2* and *UBC* were used as normalization controls. The average and SEM are represented based on eight technical replicates.

sup; see below) were more elongated than *crwn4-2* mutant nuclei, but less so than WT nuclei. In addition, nuclei in suppressed M_4 individuals contained higher numbers of distinct chromocenters compared with nuclei from the *crwn4-2* parental line (Supplemental Figure S2).

We next sought to understand the mechanism behind the restoration of these key morphological features of WT nuclei in this line. First, we examined the abundance of CRWN4 in the phenotypically suppressed line and determined that the changes in nuclear morphology were associated with an increase in CRWN4 abundance in the nucleus to approximately WT levels (Figure 5B). Therefore, the genetic change in the phenotypically suppressed line leads to normal levels of CRWN4 accumulation in nuclei, although the shape of nuclei is not fully restored.

We next investigated the nature of the underlying genetic change. The *CRWN4* gene from the suppressed line was resequenced from PCR amplicons to confirm the presence of the original *crwn4-2* mutation, thereby ruling out a true reversion event. In addition, we found no nucleotide changes in the coding region in *CRWN4* or in the region directly upstream, excluding the possibility that the line contained an intragenic suppressor mutation. These results indicated that an extragenic mutation is the most likely explanation for the observed phenotypic suppression.

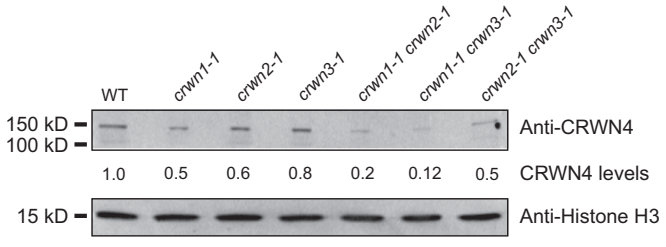

FIGURE 4: CRWN4 protein abundance across *crwn* single and double mutants. Protein immunoblots of size-fractionated nuclear extracts obtained from WT and select *crwn* single and double mutant seedlings were incubated with the antibody against CRWN4, and the protein was detected via an ECL protocol as described in Figure 2. The abundance of histone H3 was used as a normalization standard. Quantifications of the chemiluminescence signals, indicated by fractional numbers relative to WT between the blot panels, were performed using a Storm imager and ImageQuant TL software (Amersham Biosciences). This experiment is representative of blots done with independent samples from at least three independent biological replicates and additional technical replicates.

This provisional conclusion was then tested by observing the genetic behavior of the putative extragenic suppressor mutation. We crossed the putative *crwn4-2; sup* line to WT plants (outcross) as well as the nonmutagenized *crwn4-2* parental line (backcrossed). The outcrossed *CRWN4*/*crwn4-2*; *SUP*/*sup* F_1 individuals had elongated nuclei, while the *crwn4-2*/*crwn4-2*; *SUP*/*sup* F_1 individuals generated by the backcross showed partial suppression of the nuclear phenotypes. After self-pollination of the outcrossed *CRWN4*/*crwn4-2*; *SUP*/*sup* F_1 plants, we recovered individuals that had spherical nuclei characteristic of *crwn4* homozygotes. This finding demonstrates that the *sup* mutation can be segregated from the *crwn4-2* mutation and therefore lies at a separate genetic locus.

Self-pollination of backcrossed *crwn4-2*/*crwn4-2*; *SUP*/*sup* parents yielded a range of nuclear phenotypes among F_2 individuals. Plants with spherical (unsuppressed) nuclei were observed in independent F_2 families at a frequency of approximately 30%: 27 of 89 in one family and 83 of 249 in another. Among the F_2 individuals with nonspherical nuclear phenotypes, the morphology ranged from highly elongated to intermediate, making it difficult to assign precise phenotypic categories. This genetic behavior is best explained by the action of a semidominant suppressor mutation unlinked to the *crwn4-2* mutation.

To gain further insight into the mechanisms of suppression, we tested the allele specificity of the *sup* mutation. We crossed the *sup* mutation (tracked using a linked molecular marker; see below) into a background carrying the loss-of-function *crwn4-1* allele and compared the morphology of anther filament nuclei between *crwn4-1; sup* and *crwn4-2; sup* individuals, with reference to their respective parental *crwn4* strains (see Figure 5A). We found that the *sup* mutation failed to suppress the *crwn4-1* null mutation, indicating that the suppression is not due to a bypass mechanism (Guarente, 1993). Rather, the allele specificity of the *sup* mutation suggests that the suppression is mediated by a direct interaction between the product of the *sup* locus and the CRWN4 protein carrying the *crwn4-2* missense allele.

We also recovered plants carrying only the *sup* mutation in an otherwise WT background. At the whole-plant level, *CRWN4; sup* individuals are indistinguishable from WT plants; Supplemental Figure S3 shows that *CRWN4; sup* nuclei are elongated and resemble nuclei from WT plants.

Molecular identification of the *SUP* locus

Our next objective was to identify the molecular nature of the *sup* mutation. Returning to the F_2 population generated from the *crwn4-2; SUP* X *crwn4-2; sup* cross, we generated F_3 families (via self-pollination of F_2 individuals) and tested for segregation of the *sup* mutation. Six true-breeding *crwn4-2; SUP* families and three *crwn4-2; sup* families were chosen, and genomic DNA was prepared from pooled tissue for each F_3 family. Genomic libraries were then prepared for whole-genome resequencing using short-read technology. This bulked segregant approach allowed us to identify EMS-induced nonreference polymorphisms that were present in the homozygous state in the *crwn4-2; sup* pooled sample compared with reference alleles in the *crwn4-2; SUP* F_3 pool. Through this analysis, we localized the *sup* mutation to an approximately 2.5 mega base pair region on the top arm of chromosome 3. This region was defined by 18 nonreference polymorphisms in the homozygous state that affect coding sequences (listed in Supplemental Table S1).

The causal polymorphism in this region was narrowed down by genetic mapping. An expanded F_2 family (parents: *crwn4-2; SUP* X *crwn4-2; sup*) was screened and genomic DNA prepared from plants showing unsuppressed, spherical nuclear morphology (presumptive

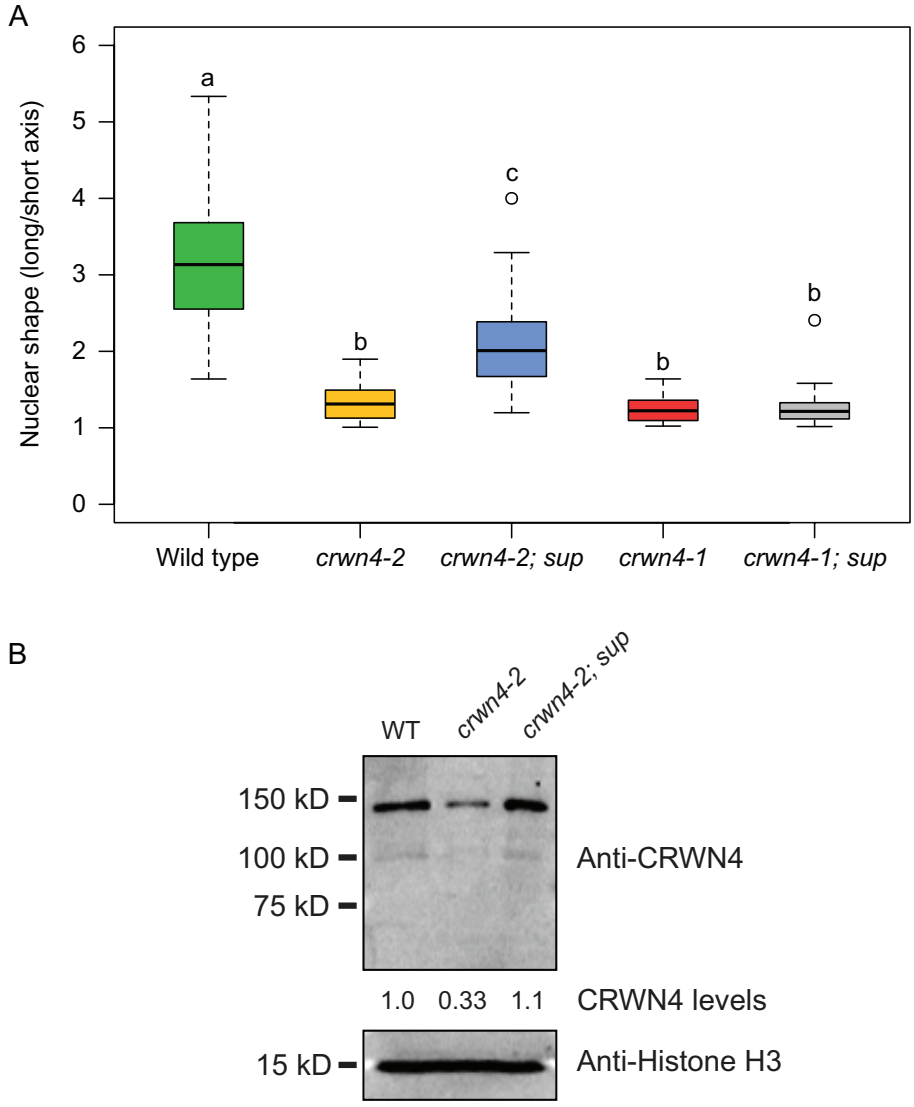

FIGURE 5: Characterization of the *crwn4-2* missense allele and an extragenic suppressor mutation. (A) Measurements of nuclear shape, expressed as the ratios of long-vs.-short axes in anther filament nuclei of different genotypes; numbers of nuclei measured: 28 (WT); 31 (*crwn4-2*); 31 (*crwn4-2; sup*); 37 (*crwn4-1*); and 41 (*crwn4-1; sup*). Central values shown are means. A one-way analysis of variance (ANOVA) Tukey honest significant difference (HSD) test was performed to identify significant differences ($p < 0.01$) among the genotypes; different lowercase letters represent genotypes that are significantly different from one another. (B) Protein immunoblots of size-fractionated nuclear extracts obtained from WT, *crwn4-2*, and *crwn4-2; sup* mutant seedlings were incubated with antibodies recognizing either CRWN4 or histone H3. After detection of the proteins using an ECL protocol, quantification of signals was performed using ImageQuant TL software (Amersham Biosciences). This experiment is representative of blots done with independent samples from three independent biological replicates.

SUP/SUP individuals). We then scored the genotype at EMS-induced polymorphic sites in these individuals and looked for strict linkage to the *SUP* genotype. As shown in Supplemental Figure S4, the *sup* mutation was delimited by recombination events to a minimal genetic window containing three nonreference alleles that altered coding regions. One mutation lies within the *PPR2* gene encoding a chloroplast protein involved in RNA editing, and another mutation causes an amino acid substitution in *At3g06480*, which encodes a DEAD-box RNA helicase implicated in nuclear RNA processing. Given their predicted roles in RNA metabolism, these EMS-induced alleles are unlikely candidates for the *sup* mutation. In contrast, the third mutation lies within the *IMPA-1* gene that codes for one of the nine isoforms of importin-α in *Arabidopsis* (Hicks *et al.*, 1996; Ballas and Citovsky, 1997). The induced G146E missense mutation in *IMPA-1* occurs between two of the protein's eight Armadillo (ARM) repeats (Figure 6) responsible for NLS recognition (Conti *et al.*, 1998). The nature of the *crwn4-2* missense allele, which alters a motif resembling an NLS, and the allele-specific behavior of the *sup* allele support the hypothesis that the *SUP* locus corresponds to *IMPA-1*.

We tested this hypothesis using a transgenic recapitulation experiment in which either a WT or a G146E version of the *IMPA-1* coding region was expressed in a *crwn4-2* mutant background. As shown in Figure 7, introduction of a transgene expressing the *impa-1* G146E allele altered the nuclear shape phenotype conferred by the *crwn4-2* mutation, but the transgenic individuals with a WT *IMPA-1* transgene had spherical nuclei characteristic of the unsuppressed *crwn4-2* mutant. Taken together, our results demonstrate that the G146E version of the IMPA-1 is able to recognize a CRWN4 protein with a K923L substitution, which destroys or severely cripples the protein's primary NLS.

DISCUSSION

Our results provide insight into the coordination between NMCP1- and NMCP2-clade proteins that work together to maintain nuclear morphology in plant cells. Here, we uncovered two mechanisms important for the nuclear accumulation of the NMCP2-type protein, CRWN4, in *Arabidopsis*. First, the abundance of CRWN4 within the nucleus depends on the presence of its NMCP1-clade paralogues. Second, we demonstrated that CRWN4 gains access to the nucleus using an NLS that can be recognized by canonical nuclear import machinery. We will consider these two mechanisms in turn, beginning with the nuclear import of CRWN4 as an example of NMCP2-type proteins.

Previous studies have established that NMCP1- and NMCP2-type proteins differ in both nuclear transport and intracellular dynamics during the cell cycle. NMCP1-type proteins contain two closely spaced monopartite NLSs in their C-terminal domain. These NLSs were identified by sequence conservation (Ciska *et al.*, 2013) as well as through functional assays for nuclear targeting (Kimura *et al.*, 2014). The latter analysis monitored the localization of transiently expressed proteins containing various forms of carrot NMCP1 (DcNMCP1) fused to a fluorescent reporter protein. Interestingly, one of these NLS regions (NLSm4) overlaps with a six-amino-acid conserved motif that is required, along with the 141 N-terminal amino acids of DcNMCP1, for targeting to the nuclear periphery. NMCP2 proteins lack this six-amino-acid motif and the flanking

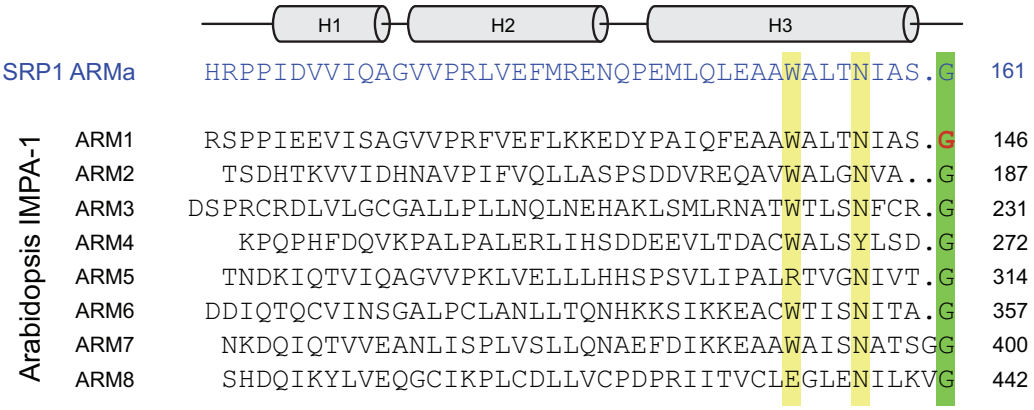

FIGURE 6: The position of the missense mutation in *IMPA-1* corresponds to the NLS-recognition region in yeast importin-α (SRP1). The amino acid sequences of the eight ARM repeats of the *Arabidopsis* IMPA-1 protein are aligned under the corresponding sequence of the yeast importin-α SRP1 (blue text). The alpha helices of the yeast SRP1 ARMa repeat are depicted at the top, and the conserved tryptophan (W) and asparagine (N) residues in helix 3 are highlighted in yellow (Conti *et al.*, 1998; Chang *et al.*, 2012). The green bar marks the position of mutated glycine (G) residue (#146), which is shown in red. The amino acid coordinates are shown to the right of the sequences.

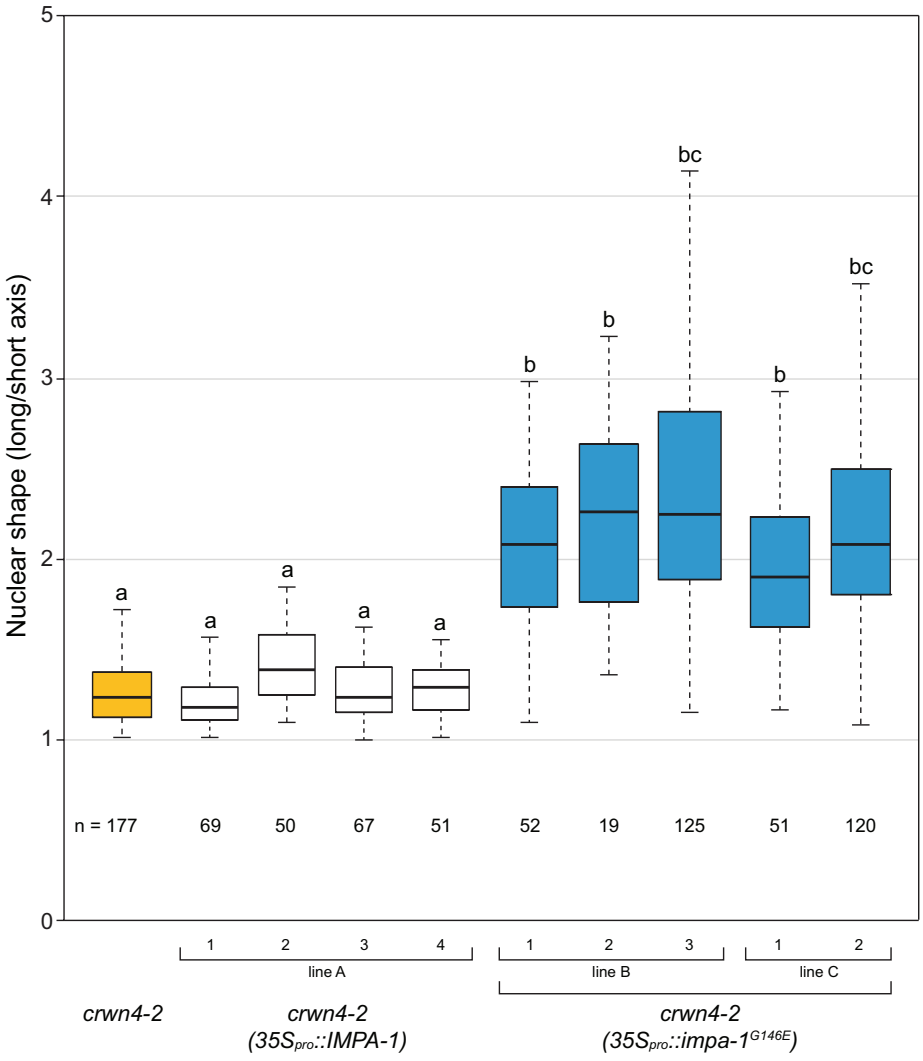

FIGURE 7: Expression of *impa-1*^{G146E}, but not WT *IMPA-1*, suppresses the nuclear shape phenotype in *crwn4-2* mutants. Transgene constructs expressing either the WT *IMPA-1* coding sequence or the *impa-1*^{G146E} coding sequence under control of the strong CaMV 35S promoter were introduced into *crwn4-2* mutants. Anther filament nuclei were examined from a *crwn4-2* mutant lacking a transgene or different individuals from three transgenic lines: line A carrying an *IMPA-1* transgene or lines B and C carrying an *impa-1*^{G146E} transgene. Measurements of nuclear shape, expressed as the ratios of long-vs.-short axes are shown; numbers of nuclei measured are indicated by *n* = # toward the bottom of the graph. Central values shown are medians. A one-way ANOVA Tukey HSD test was performed; samples that do not share a lowercase letter are significantly different from one another ($p < 0.01$).

NLSs (Kimura *et al.*, 2010, 2014). Further, the N-terminal domain of DcNMCP2 cannot substitute for the N-terminal region of DcNMCP1 in the targeting assay for nuclear rim localization (Kimura *et al.*, 2014). Perhaps related to these structural differences, the intracellular dynamics of carrot NMCP1 and NMCP2 during nuclear reformation in mitosis are distinct (Kimura *et al.*, 2010). After the onset of nuclear membrane breakdown in prometaphase, much of the pool of DcNMCP1 associates with the mitotic spindle and then shifts to the surface of chromatin starting in anaphase. In contrast, DcNMCP2 disperses after prometaphase into the mitotic cytoplasm and then associates with putative nuclear membrane vesicles before accumulating at the surface of chromatin at early telophase. Despite these differences, NMCP2-type proteins, like *Arabidopsis* CRWN4, need to be transported into the nucleus, and their lack of a conspicuous NLS initially led us, and others

(Kimura *et al*., 2010), to consider the possibility that these proteins associate with their NLS-containing paralogues or unrelated proteins to gain access to the nucleus via a cotransport mechanism (Fabbro *et al*., 2002; Knudsen *et al*., 2009).

Two key findings from the present work, however, indicate that CRWN4 does contain a functional NLS that can be recognized by nuclear transport machinery. First, the *crwn4-2* missense allele alters a short stretch of basic amino acids that scores in prediction algorithms as a possible monopartite NLS (Figure 1D). The amino acid substitution, which is predicted to destroy the NLS, leads to a 60–70% reduction in the levels of CRWN4 in the nucleus (Figure 5B). The second line of evidence is the identification of a missense mutation in the *IMPA-1* gene, encoding an isoform of importin-α, as an allele-specific suppressor of the *crwn4-2* mutation that restores the level of nuclear CRWN4 (Figures 5 and 7). The *IMPA-1* mutation (G146E) occurs at the junction between the first and second of eight tandem Armadillo (ARM) repeats, and the altered glycine corresponds to a residue conserved in other importin-α proteins in fungi and animals (Conti *et al*., 1998). More precisely, the G146E substitution falls in a region at the boundary of helix 3 in ARM repeat 1 close to the conserved WxxxN pairs in helix 3 that form the floor of the hydrophobic groove that orients and interacts with the NLS on transport cargoes (Figure 6). Further, the G146E substitution lies in a region corresponding to the superhelix of yeast importin-α (SRP1) that interacts with the core KKxK motif in classical monopartite NLSs (Conti *et al*., 1998). These considerations support a model in which the altered IMPA-1 protein gains the ability to interact with the altered *crwn4-2* NLS motif, or possibly with an alternative cryptic NLS in CRWN4, thereby allowing nuclear entry and restoration of normal levels of protein in the nucleus (Figure 5B). Notably, full CRWN4 function is often not completely restored in *crwn4-2; sup* individuals (see Figure 5A), suggesting either that the nuclear CRWN4 pool is not assembled or that the *crwn4-2* mutation might partially disrupt the function of protein within the nucleus.

Our findings highlight some important open questions. First, it is not known whether IMPA-1 is the importin-α isoform that normally recognizes CRWN4. One possible scenario is that the WT version of IMPA-1 does not recognize CRWN4, but the G146E mutation allows interaction with CRWN4 carrying the altered NLS (i.e., *impa-1*^{G146E} is a neomorphic mutation enabling recognition of novel transport cargoes). A second question is whether or not CRWN4 relies completely on the discovered monopartite NLS for nuclear import. The residual amount of nuclear CRWN4 detected in *crwn4-2* mutants (approximately 30%) could be due to less efficient import mediated via a weaker secondary NLS. Alternatively, some CRWN4 might gain entry into the nucleus via an alternative pathway, such as the previously hypothesized coimport mechanism.

The identification of a functional NLS in CRWN4 allowed us to investigate the conservation of this motif in its orthologues. As shown in Supplemental Figure S5, a related NLS is evident in orthologues from related taxa, but the motif is not recognizable in NMCP2 proteins from more distantly related plants. Some sense of the relative divergence of NLS motifs can be gained by examining the situation in dicot *Daucus carota* (carrot), where the prototypic NMCPs were first discovered and studied. The functional NLSm3 and NLSm4 sequences in DcNMCP1 identified by Kimura *et al*. (2014) are still recognizable in the three *Arabidopsis* NMCP1-type proteins (Kimura *et al*., 2014) (see Figure 1C). In contrast, the NLS identified in this study is not conserved between NMCP2 orthologues in carrot and *Arabidopsis*. However, a potential alternative bipartite NLS motif exists in DcNMCP2 nearby, which also corresponds to the general position of the NLS motifs in NMCP1-type proteins (see Figure 1A and Supplemental Figure S5). Interestingly, a candidate bipartite NLS is found in NMCP2 orthologues in monocot taxa (represented in Supplemental Figure S5 by the grasses rice and maize) at a position that overlaps the NLS discovered in this study. Therefore, it is likely that nuclear import of NMCP2 proteins relies on rapidly evolving NLS sequences whose amino acid identity is divergent but whose position in the protein is conserved.

We turn now to the other mechanism uncovered in this study that regulates the abundance of NMCP2-type proteins in the nucleus. Once imported into the nucleus, the level of CRWN4 is affected by the presence or absence of its paralogues in the NMCP1 family. As shown in Figure 2, the abundance of CRWN4 in the nucleus is decreased in the absence of either CRWN1 or CRWN3. Further, the decrease is accentuated by the deficiency of two NMCP1-type paralogues (Figure 4), provided that CRWN1 is one of the absent paralogues. Steady-state *CRWN4* transcript levels are not affected by mutations in the other *crwn* genes (Figure 3), suggesting that the effects on CRWN4 abundance occur at the posttranscriptional or protein level.

We propose two different models to explain these results. The first posits that CRWN4 is stabilized in the nucleus in complexes with its NMCP1-clade paralogues. Two published reports indicate that CRWN1 and CRWN4 can be coimmunoprecipitated along with other targeted proteins (Goto *et al*., 2014; Mikulski *et al*., 2019). These findings demonstrate that CRWN4 interacts with CRWN1 but do not distinguish between direct and indirect physical interactions. Direct interaction could occur at the level of heterodimer formation mediated by the long coiled-coil domains, analogous to the observed dimerization of lamin monomers (de Leeuw *et al*., 2018) (although recent in vivo imaging argues that tetramers might be the fundamental aggregate form [Turgay *et al*., 2017]). Alternatively, interaction could be indirect and result from coimmunoprecipitation of large macromolecular complexes containing CRWN4 aggregates and distinct CRWN1 aggregates. The available data in animals suggest that the different lamin subtypes (A/C and B) form separate filament lattices in the nuclear lamina (Goldberg *et al*., 2008; Shimi *et al*., 2008, 2015; Turgay *et al*., 2017). An immunolocalization study in onion uncovered distinct microdomains that contain predominantly NMCP1 or NMCP2 proteins, suggesting that the plant nuclear lamina might contain distinct lattice subtypes (Ciska *et al*., 2018). Regardless of the specifics of the physical interactions, any type of complex formation involving CRWN1 and CRWN4 could explain why loss of one protein could lead to increased turnover of the unbound partner monomer or aggregate. One prediction of this simple model is that the effects should be reciprocal; however, while CRWN4 levels change significantly in the absence of CRWN1, the converse is not true. This consideration points to an alternative model involving more complex regulation among NMCP1- and NMCP2-type proteins in plant nuclei. In this scenario, CRWN1 and CRWN4 complexes might be independent but interrelated, through either structural connections or regulatory intermediaries. Evidence for cross-talk among nuclear lamina subtypes was reported in mammalian cells (Shimi *et al*., 2008, 2015). For example, after knocking down expression of lamin B1 using short-hairpin RNA in HeLa cells, these authors observed an alteration in the pore size of both lamin A and lamin B2 networks and the mobility of the nucleoplasmic fraction of lamin A (Shimi *et al*., 2008). By analogy, it is possible that NMCP2 networks might be altered and destabilized by changes in the amount of NMCP1-type proteins or by the absence of specific isoforms. Elucidating the specific mechanisms that underlie the cross-regulation, which we have demonstrated here, between NMCP1- and NMCP2-type proteins promises to uncover the full

complexity of the composition and function of the plant nuclear lamina.

MATERIALS AND METHODS

Request a protocol through Bio-protocol.

Plant materials and growth conditions

Arabidopsis thaliana ecotype Columbia was used as the WT. The *crwn1-1*, *crwn2-1*, *crwn3-1*, *crwn4-1*, *crwn1-1 crwn2-1*, *crwn1-1 crwn3-1*, and *crwn2-1 crwn3-1* mutants used in this study were previously described (Wang *et al.*, 2013). The *crwn4-2* missense allele was discovered in a genetic screen utilizing a fast neutron mutagenesis to search for novel abnormal nuclear morphology mutants. The environmental growth chamber used in these studies were set to long-day conditions with a 16-h light/8-h dark period at approximately 23°C and 60% relative humidity.

For protein extraction, approximately 50 seeds were sterilized in 50% (vol/vol) bleach solution and washed at least three times with sterile MilliQ water. Aseptic seeds were added to Murashige and Skoog (MS) media supplemented with 1% sucrose and 1× Gamborg's Vitamin solution and were grown under continuous shaking conditions at room temperature in the dark for 11 d. For qRT-PCR analysis, aseptic seeds were placed on petri dishes containing MS agar supplemented with 10 g/l sucrose. Following an incubation at 4°C for 2 d in the dark, the plates were transferred to the environmental growth chamber. For microscopic imaging, seeds were grown on MetroMix 360+ soil in the environmental growth chamber.

Antibody preparation

Antipeptide polyclonal antibodies recognize the N-terminal regions of CRWN1 and CRWN4, respectively. Peptide antigens (CRWN1: MSTPLKVWQRWSTPT; CRWN4: RSERFPITPSTAATNRLT) were synthesized and injected into rabbits by Proteintech (Rosemont, IL), a commercial antiserum production company, to raise the corresponding antisera, which were then affinity purified.

Nuclear protein extraction and Western blot analysis

For nuclear protein extractions, seedlings were harvested and homogenized thoroughly in cold Honda buffer (0.44 M sucrose,1.25% Ficoll, 2.5% Dextran T40, 20 mM HEPES-KOH, pH 7.4, 10 mM $MgCl_2$, 0.5% Triton X-100) with a Protease inhibitor cocktail using mortar and pestle. The resulting homogenate was filtered through two layers of nylon mesh (Membrane Solutions) with the top layer having a pore size of 100 µm and the bottom layer having a pore size of 20 µm. The clear liquid phase was centrifuged at 7000 rpm for 30 min at 4°C to obtain the nuclear pellet. The pellet was then washed three times using Honda buffer (without Protease inhibitor cocktail) until the pellet turned gray. The nuclear pellet was either kept on ice for immediate analysis by Western blot or stored at –20°C.

After the nuclear pellets were resuspended in 2× Laemmli buffer (1.6% SDS, 20% glycerol, 120 mM Tris, 0.02% bromphenol blue) with 10% β-mercaptoethanol, the samples were boiled for 5 min and resolved on a 10% separating gel via SDS–PAGE. The gel was then transferred to a nylon membrane (Amersham Biosciences) using electroblot transfer systems. After the membrane was blocked at 4°C, the blot was probed with either anti-CRWN1 or anti-CRWN4 primary antibody solutions diluted at 1:1000, followed by an incubation in anti-rabbit horseradish peroxidase (HRP)-conjugated secondary antibody solutions. Proteins were detected using ECL Plus Substrate (Thermo Scientific/Pierce) and a Storm imager (Amersham Biosciences) and their abundance quantified using ImageQuant TL software (Amersham Biosciences).

RNA isolation, cDNA preparation, and qRT-PCR analysis

RNA was extracted using the E.Z.N.A. Plant RNA Kit (Omega Biotek) after collecting 50 seedlings from each selected genotype. Following a treatment with DNase 1 (New England Biolabs), cDNA was synthesized via the SuperScript IV First-Strand Synthesis System (Invitrogen). To examine transcript levels of *CRWN4*, qRT-PCR was performed for WT and the *crwn* single mutants with primers RT-CRWN4-F (5′-TTGTGTCTCGGGATGATGAA-3′) and RT-CRWN4-R (5′-AAGGGGTTAAGCCGTTCTGT-3′), using iTaq Universal SYBR Green Supermix (BioRad) on a BioRad C1000 thermal cycler for 40 cycles. *ACTIN2* and *UBC* were used as endogenous controls to normalize the samples using the primers specified by Czechowski *et al.* (2005).

Microscopic imaging

Anther filaments of flowering plants were first fixed in a 3:1 ethanol: acetic acid solution for at least 20 min. Following a rinse in water, the filaments were briefly dipped in DAPI working solution (at 1 µg/ml) and then in water and placed on a slide for imaging using a Leica DM5500 epifluorescence microscope.

crwn4-2 suppressor screening

The starting material for this screen was an *A. thaliana* Columbia strain homozygous for the *crwn4-2* allele and an NLS-GFP-GUS transgene, which encodes a GFP fused to a plant nuclear localization signal (NLS) and to β-glucuronidase (GUS) from E*scherichia coli*, expressed under a constitutive CaMV 35S promoter (Chytilova *et al.*, 1999). This transgene marker allows for nuclei to be imaged in live seedling tissues, and the *crwn4-2* allele was one of 11 mutations we recovered from a fast-neutron mutagenesis looking for variants with spherical root cell nuclei. The *crwn4-2* mutation, a base-pair substitution affecting a pyrimidine dinucleotide site (5′-TpT-3′/5′-ApA-3′), conforms with the known mutagenic spectrum of fast neutrons (Belfield *et al.*, 2012). To generate mutations that might suppress the *crwn4-2* phenotype, the seeds were treated with the alkylating agent EMS, and the resulting M_1 plants self-pollinated to segregate mutations. Seedlings in the next generation (M_2) were screened for elongated nuclei in root cells to identify plants containing reversions or suppressor mutations. For screening, M_2 seeds were grown on 1× MS agar plates with 1% sucrose and 0.7% phytoagar, cold-treated at 4°C overnight for stratification, and grown vertically in the environmental growth chamber. After 1 wk of growth, the roots were phenotyped using a Leica M205 fluorescence stereomicroscope. WT and nonmutagenized *crwn4-2* seeds were also grown as controls. Candidate suppressor seedlings were transplanted from the MS plates to soil and returned to the environmental growth chamber. Once these plants began flowering, anther filaments were harvested, DAPI stained, and imaged as described above to observe whether or not the nuclear root phenotype observed in the seedling was present in adult tissues. M_3 seed was generated from the candidate suppressor line to test for transmission to the next generation and subsequent molecular analysis and genetic crosses. Using the urea lysis miniprep protocol (Cocciolone and Cone, 1993), genomic DNA was extracted from candidate and control plants. Genotyping for the presence or absence of the original *crwn4-2* allele was performed by standard PCR using GoTaq DNA polymerase (Promega) and either a4WTF 5′-TGAGACTAGCGAACCAAGCAATAACAA-3′ or a4MutF 5′-TGAGACTAGCGAACCAAGCAATAACCT-3′ with a41kbR2 5′-TCCAGCCGAACACTCTTGCTGTTG-3′, where primer pair a4WTF/a41kbR2 recognizes the WT *CRWN4* sequence while primer pair a4MutF/a41kbR2 includes the *crwn4-2* point mutation (the dinucleotide change corresponds

to the 3′ end of the a4MutF primer). In addition, we determined the entire *CRWN4* genomic sequence in the *crwn4-2; sup* individual, from PCR amplicon templates, to confirm the presence of the original *crwn4-2* missense allele, as well as to rule out the existence of potential intragenic suppressor mutations.

Genetic mapping of the *SUP* locus

A bulked-segregant analysis combined with whole-genome resequencing was performed on two F_3 pooled genomic DNA preps comparing *crwn4-2/crwn4-2*; *SUP/SUP* versus *crwn4-2/crwn4-2*; *sup/sup* genotypes (the genetic crosses generating this material are described in detail in *Results*). DNA sequencing libraries were constructed by Polar Genomics (Ithaca, NY), and reads were generated in Cornell University's Institute of Biotechnology sequencing core using Illumina NextSeq technology. The reads were aligned to the reference Columbia genome sequence (Arabidopsis Genome Initiative, 2000) and nonreference alleles identified using the Genome Analysis Toolkit suite developed by the Broad Institute (McKenna *et al.*, 2010). EMS-induced mutations that affected protein-coding genes were identified using the SNPEff tool (Cingolani *et al.*, 2012). The critical region containing the *SUP* locus was identified by a segment of chromosome 3 that was enriched for loci that were homozygous for nonreference alleles in the *crwn4-2/crwn4-2*; *sup/sup* sample and for reference alleles in the *crwn4-2/crwn4-2*; *SUP/SUP* sample (see Supplemental Table S1). Genetic fine mapping was conducted by genotyping approximately 100 F_2 individuals (from a self-pollinated *crwn4-2/crwn4-2*; *SUP/sup* parent) that contained spherical/ovoid nuclei (i.e., *SUP/SUP* individuals) using PCR-based markers developed to distinguish between reference and nonreference alleles.

Suppressor transgenic recapitulation experiment

The coding sequence of the *IMPA-1* gene or the *impa-1*^{G146E} allele was amplified from genomic templates using a high-fidelity thermostable DNA polymerase (Phusion; New England Biolabs) and primers IMPA-1_dTF1: 5′-CACCTACATTAGCTTGCCTCAAAGAACAC-3′ and IMPA1_ORF_R2: 5′-TCAGCTGAAGTTGAATCCTCCGGAT-3′. The amplified regions contained all exons (including the stop codon) and introns, the annotated 5′-UTR and an additional 167 base pairs upstream. These amplification products were inserted into Gateway entry vector (pENTR/D-TOPO) using directional TOPO cloning (Invitrogen/Life Technologies). Sequence-verified inserts were moved via LR Clonase reactions (Invitrogen/Life Technologies) into the Gateway destination vector pEG100 (Earley *et al.*, 2006), which contains T-DNA borders for *Agrobacterium*-mediated plant transformation, a Cauliflower Mosaic Virus 35S promoter to amplify expression, and an OCS 3′ end. Validate constructs were then electroporated into *Agrobacterium* strain LBA4404, and *crwn4-2* mutant plants were transformed using the floral dip method (Bent, 2006). Transformants were identified among the progeny by selection for resistance to the herbicide Basta (glufosinate).

Additional computational analysis

In determining the coiled-coil domains of the CRWN proteins, sequences were analyzed using the MARCOIL program (Delorenzi and Speed, 2002; Zimmermann *et al.*, 2018). Alignments of CRWN protein sequences were performed using the Clustal Omega program (version 1.2.4; Sievers *et al.*, 2011). For NLS motif analysis, cNLS Mapper was used on the entire sequence with a cutoff score of 5.0 (Kosugi *et al.*, 2009b).

ACKNOWLEDGMENTS

We are grateful for the facilities provided by the Boyce Thompson Institute's Plant Cell Imaging Center and Plant Growth Facility. We thank Junsik Choi, Leila Feiz, Molly Shook, and Mamta Srivastava for technical advice, helpful comments, and discussion. We are grateful to Julia Vrebalov for sequencing library construction and the BTI Computational Biology Center for help with bioinformatics analysis, with a special thanks to Yi Zheng and Susan Strickler for their advice and support. We acknowledge the work of Travis Dittmer and Haiyi Wang in developing the antibody reagents. The T-DNA mutant alleles used in this study were originally obtained from the Arabidopsis Biological Resource Center at The Ohio State University. This work was supported by funds provided by the Boyce Thompson Institute, the Triad Foundation, and a grant (URoL-2022048) to E.J.R. from the National Science Foundation. In addition, E.L.B. received fellowship support from Cornell University.

REFERENCES

Arabidopsis Genome Initiative. (2000). Analysis of the genome sequence of the flowering plant *Arabidopsis thaliana*. Nature 408, 796–815.

Ballas N, Citovsky V (1997). Nuclear localization signal binding protein from Arabidopsis mediates nuclear import of agrobacterium VirD2 protein. Proc Natl Acad Sci USA 94, 10723–10728.

Belfield EJ, Gan X, Mithani A, Brown C, Jiang C, Franklin K, Alvey E, Wibowo A, Jung M, Bailey K, *et al.* (2012). Genome-wide analysis of mutations in mutant lineages selected following fast-neutron irradiation mutagenesis of Arabidopsis thaliana. Genome Res 22, 1306–1315.

Bent A (2006). Arabidopsis thaliana floral dip transformation method. Methods Mol Biol 343, 87–103.

Chang CW, Couñago RL, Williams SJ, Boden M, Kobe B (2012). Crystal structure of rice importin-alpha and structural basis of its interaction with plant-specific nuclear localization signals. Plant Cell 24, 5074–5088.

Choi J, Strickler SR, Richards EJ (2019). Loss of CRWN nuclear proteins induces cell death and salicylic acid defense signaling. Plant Physiol 179, 1315–1329.

Chytilova E, Macas J, Galbraith DW (1999). Green fluorescent protein targeted to the nucleus, a transgenic phenotype useful for studies in plant biology. Ann Bot 83, 645–654.

Cingolani P, Platts A, Wang LL, Coon M, Nguyen T, Wang L, Land SJ, Lu XY, Ruden DM (2012). A program for annotating and predicting the effects of single nucleotide polymorphisms, SnpEff: SNPs in the genome of *Drosophila melanogaster* strain *w(1118); iso-2; iso-3*. Fly 6, 80–92.

Ciska M, Hikida R, Masuda K, Moreno Diaz de la Espina S (2019). Evolutionary history and structure of nuclear matrix constituent proteins, the plant analogues of lamins. J Exp Bot 70, 2651–2664.

Ciska M, Masuda K, Moreno Diaz de la Espina S (2013). Lamin-like analogues in plants: the characterization of NMCP1 in *Allium cepa*. J Exp Bot 64, 1553–1564.

Ciska M, Masuda K, Moreno Diaz de la Espina S (2018). Characterization of the lamin analogue NMCP2 in the monocot *Allium cepa*. Chromosoma 127, 103–113.

Cocciolone SM, Cone KC (1993). *Pl-Bh*, an anthocyanin regulatory gene of maize that leads to variegated pigmentation. Genetics 135, 575–588.

Conti E, Uy M, Leighton L, Blobel G, Kuriyan J (1998). Crystallographic analysis of the recognition of a nuclear localization signal by the nuclear import factor karyopherin alpha. Cell 94, 193–204.

Crisp M, Liu Q, Roux K, Rattner JB, Shanahan C, Burke B, Stahl PD, Hodzic D (2006). Coupling of the nucleus and cytoplasm: role of the LINC complex. J Cell Biol 172, 41–53.

Czechowski T, Stitt M, Altmann T, Udvardi MK, Scheible WR (2005). Genome-wide identification and testing of superior reference genes for transcript normalization in Arabidopsis. Plant Physiol 139, 5–17.

Dechat T, Pfleghaar K, Sengupta K, Shimi T, Shumaker DK, Solimando L, Goldman RD (2008). Nuclear lamins: major factors in the structural organization and function of the nucleus and chromatin. Genes Dev 22, 832–853.

de Leeuw R, Gruenbaum Y, Medalia O (2018). Nuclear lamins: thin filaments with major functions. Trends Cell Biol 28, 34–45.

Delorenzi M, Speed T (2002). An HMM model for coiled-coil domains and a comparison with PSSM-based predictions. Bioinformatics 18, 617–625.

Dittmer TA, Richards EJ (2008). Role of LINC proteins in plant nuclear morphology. Plant Signal Behav 3, 485–487.

Dittmer TA, Stacey NJ, Sugimoto-Shirasu K, Richards EJ (2007). *LITTLE NUCLEI* genes affecting nuclear morphology in *Arabidopsis thaliana*. Plant Cell 19, 2793–2803.
Earley KW, Haag JR, Pontes O, Opper K, Juehne T, Song K, Pikaard CS (2006). Gateway-compatible vectors for plant functional genomics and proteomics. Plant J 45, 616–629.
Fabbro M, Rodriguez JA, Baer R, Henderson BR (2002). BARD1 induces BRCA1 intranuclear foci formation by increasing RING-dependent BRCA1 nuclear import and inhibiting BRCA1 nuclear export. J Biol Chem 277, 21315–21324.
Goldberg MW, Huttenlauch I, Hutchison CJ, Stick R (2008). Filaments made from A- and B-type lamins differ in structure and organization. J Cell Sci 121, 215–225.
Goto C, Tamura K, Fukao Y, Shimada T, Hara-Nishimura I (2014). The novel nuclear envelope protein KAKU4 modulates nuclear morphology in Arabidopsis. Plant Cell 26, 2143–2155.
Gruenbaum Y, Margalit A, Goldman RD, Shumaker DK, Wilson KL (2005). The nuclear lamina comes of age. Nat Rev Mol Cell Biol 6, 21–31.
Guarente L (1993). Synthetic enhancement in gene interaction: a genetic tool come of age. Trends Genet 9, 362–366.
Hicks GR, Smith HMS, Lobreaux S, Raikhel NV (1996). Nuclear import in permeabilized protoplasts from higher plants has unique features. Plant Cell 8, 1337–1352.
Horn HF (2014). LINC complex proteins in development and disease. Curr Top Dev Biol 109, 287–321.
Kimura Y, Fujino K, Ogawa K, Masuda K (2014). Localization of *Daucus carota* NMCP1 to the nuclear periphery: the role of the N-terminal region and an NLS-linked sequence motif, RYNLRR, in the tail domain. Front Plant Sci 5, 62.
Kimura Y, Kuroda C, Masuda K (2010). Differential nuclear envelope assembly at the end of mitosis in suspension-cultured *Apium graveolens* cells. Chromosoma 119, 195–204.
Knudsen NO, Andersen SD, Lutzen A, Nielsen FC, Rasmussen LJ (2009). Nuclear translocation contributes to regulation of DNA excision repair activities. DNA Repair 8, 682–689.
Kosugi S, Hasebe M, Matsumura N, Takashima H, Miyamoto-Sato E, Tomita M, Yanagawa H (2009a). Six classes of nuclear localization signals specific to different binding grooves of importin alpha. J Biol Chem 284, 478–485.
Kosugi S, Hasebe M, Tomita M, Yanagawa H (2009b). Systematic identification of cell cycle-dependent yeast nucleocytoplasmic shuttling proteins by prediction of composite motifs. Proc Natl Acad Sci USA 106, 10171–10176.
Lammerding J (2011). Mechanics of the nucleus. Compr Physiol 1, 783–807.
Lammerding J, Schulze PC, Takahashi T, Kozlov S, Sullivan T, Kamm RD, Stewart CL, Lee RT (2004). Lamin A/C deficiency causes defective nuclear mechanics and mechanotransduction. J Clin Invest 113, 370–378.
Masuda K, Haruyama S, Fujino K (1999). Assembly and disassembly of the peripheral architecture of the plant cell nucleus during mitosis. Planta 210, 165–167.
Masuda K, Takahashi S, Nomura K, Arimoto M, Inoue M (1993). Residual structure and constituent proteins of the peripheral framework of the cell-nucleus in somatic embryos from *Daucus carota* L. Planta 191, 532–540.
Masuda K, Xu ZJ, Takahashi S, Ito A, Ono M, Nomura K, Inoue M (1997). Peripheral framework of carrot cell nucleus contains a novel protein predicted to exhibit a long alpha-helical domain. Exp Cell Res 232, 173–181.
McKenna A, Hanna M, Banks E, Sivachenko A, Cibulskis K, Kernytsky A, Garimella K, Altshuler D, Gabriel S, Daly M, DePristo MA (2010). The Genome Analysis Toolkit: a MapReduce framework for analyzing next-generation DNA sequencing data. Genome Res 20, 1297–1303.
Meier I, Richards EJ, Evans DE (2017). Cell biology of the plant nucleus. Annu Rev Plant Biol 68, 139–172.
Mikulski P, Hohenstatt ML, Farrona S, Smaczniak C, Stahl Y, Kalyanikrishna Kaufmann, K, Angenent G, Schubert D (2019). The chromatin-associated protein PWO1 interacts with plant nuclear amin-like components to regulate nuclear size. Plant Cell 31, 1141–1154.
Padmakumar VC, Libotte T, Lu W, Zaim H, Abraham S, Noegel AA, Gotzmann J, Foisner R, Karakesisoglou I (2005). The inner nuclear membrane protein Sun1 mediates the anchorage of Nesprin-2 to the nuclear envelope. J Cell Sci 118, 3419–3430.
Poulet A, Probst AV, Graumann K, Tatout C, Evans D (2017). Exploring the evolution of the proteins of the plant nuclear envelope. Nucleus 8, 46–59.
Sakamoto Y, Takagi S (2013). LITTLE NUCLEI 1 and 4 regulate nuclear morphology in *Arabidopsis thaliana*. Plant Cell Physiol 54, 622–633.
Shimi T, Kittisopikul M, Tran J, Goldman AE, Adam SA, Zheng YX, Jaqaman K, Goldman RD (2015). Structural organization of nuclear lamins A, C, B1, and B2 revealed by superresolution microscopy. Mol Biol Cell 26, 4075–4086.
Shimi T, Pfleghaar K, Kojima SI, Pack CG, Solovei I, Goldman AE, Adam SA, Shumaker DK, Kinjo M, Cremer T, Goldman RD (2008). The A- and B-type nuclear lamin networks: microdomains involved in chromatin organization and transcription. Gene Dev 22, 3409–3421.
Sievers F, Wilm A, Dineen D, Gibson TJ, Karplus K, Li WZ, Lopez R, McWilliam H, Remmert M, Soding J, *et al.* (2011). Fast, scalable generation of high-quality protein multiple sequence alignments using Clustal Omega. Mol Syst Biol 7, 539.
Turgay Y, Eibauer M, Goldman AE, Shimi T, Khayat M, Ben-Harush K, Dubrovsky-Gaupp A, Sapra KT, Goldman RD, Medalia O (2017). The molecular architecture of lamins in somatic cells. Nature 543, 261–264.
Wang H, Dittmer TA, Richards EJ (2013). Arabidopsis CROWDED NUCLEI (CRWN) proteins are required for nuclear size control and heterochromatin organization. BMC Plant Biol 13, 200.
Zimmermann L, Stephens A, Nam SZ, Rau D, Kubler J, Lozajic M, Gabler F, Soding J, Lupas AN, Alva V (2018). A completely reimplemented MPI bioinformatics toolkit with a new HHpred server at its core. J Mol Biol 430, 2237–2243.

ETOC:

NMCP proteins with extended coiled-coil domains are major structural components of the nucleoskeleton in plant cells. We show that the three NMCP1-type proteins in *Arabidopsis* maintain the nuclear pool of the single NMCP2-type protein, which gains access to the nucleus through interaction with the importin-α isoform, IMPA-1.